Thermodynamic characterization of an engineered tetracycline-binding riboswitch

Michael Müller, Julia E. Weigand, Oliver Weichenrieder[1] and Beatrix Suess*

Lehrstuhl für Mikrobiologie, Friedrich-Alexander-Universität Erlangen-Nürnberg, Staudtstrasse 5,
91058 Erlangen, Germany and [1]The Netherlands Cancer Institute, Department of Molecular Carcinogenesis,
Plesmanlaan 121, 1066 CX, Amsterdam, The Netherlands

ABSTRACT

Riboswitches reflect a novel concept in gene regulation that is particularly suited for technological adaptation. Therefore, we characterized thermodynamically the ligand binding properties of a synthetic, tetracycline (tc)-binding RNA aptamer, which regulates gene expression in a dose-dependent manner when inserted into the untranslated region of an mRNA. *In vitro*, one molecule of tc is bound by one molecule of partially pre-structured and conformationally homogeneous apo-RNA. The dissociation constant of 770 pM, as determined by fluorimetry, is the lowest reported so far for a small molecule-binding RNA aptamer. Additional calorimetric analysis of RNA point mutants and tc derivatives identifies functional groups crucial for the interaction and including their respective enthalpic and entropic contributions we can propose detailed structural and functional roles for certain groups. The conclusions are consistent with mutational analyses *in vivo* and support the hypothesis that tc-binding reinforces the structure of the RNA aptamer, preventing the scanning ribosome from melting it efficiently.

INTRODUCTION

Gene regulation at the level of RNA frequently exploits the conformational flexibility and functional versatility of this macromolecule and has been a field of intense research in the past few years. One of the most recent discoveries are natural riboregulators that control a wide set of metabolic pathways in prokaryotes [reviewed in (1–4)]. These molecular switches, also called riboswitches, consist solely of RNA and undergo structural transformations, for example in response to the level of specific small metabolites, which are bound directly by the RNA. Conformational changes within riboswitches that are part of protein-coding RNAs lead to a modulated expression of the respective gene via mechanisms like transcriptional attenuation, inhibition of translation initiation or ribozyme-mediated mRNA degradation.

Mechanistically, riboswitches are exceptional. They fulfill both sensory and regulatory functions in one and are physically part of the regulated target RNA. Separate, protein-based sensors and regulators that would act *in trans* are thus not required. These distinct principles provide an ideal and novel platform for the development of powerful tools in the field of gene regulation. Rational design, *in vitro* selection and *in vivo* screening systems [reviewed in (5,6)] have resulted in a versatile set of RNA-based molecular switches, which are small and universally applicable. They respond in a dose-dependent way to small, ideally non-metabolic molecules that are taken up well by the cell without being toxic.

One approach to develop artificial riboswitches is based on RNA aptamers. These are synthetic, *in vitro* selected RNA molecules with outstanding affinity and specificity for their respective target. Usually, they adopt a unique conformation only upon ligand binding, with the ligand becoming an integral part of the complex (7,8). This conformational change was exploited in the development of conditional gene regulation systems by inserting aptamers into the 5′-untranslated region (5′-UTR) of eukaryotic mRNA, where the aptamer–ligand complex interferes with initial stages of translation initiation (9–11). In this context, we have identified an aptamer that binds tetracycline (tc) and that can be used in yeast for tc-dependent regulation of gene expression (11). When this aptamer is placed close to the cap structure, the tc aptamer complex prevents the recruitment of the small ribosomal subunit. Furthermore, the complex also interferes with the formation of the 80S ribosome when inserted in front of the start codon, probably by blocking the small ribosomal subunit from scanning through the 5′-UTR (12). Chemical and

*To whom correspondence should be addressed. Tel: +49 9131 852 88 18; Fax: +49 9131 852 80 82; Email: bsuess@biologie.uni-erlangen.de
*Correspondence may also be addressed to Oliver Weichenrieder. Tel: +31 20 512 1951; Fax: +31 20 512 1954; Email: o.weichenrieder@nki.nl

enzymatic probing and mutagenesis studies revealed large parts of the aptamer to be affected by ligand binding and have led to a hypothesis in which binding of tc to the aptamer induces or stabilizes tertiary contacts within the RNA as the molecular basis for regulation (13).

Many natural riboswitches are relatively large and only poorly characterized from a thermodynamic point of view. In contrast, the present tc-dependent riboswitch is one of the smallest known and has been studied over several years. It turned out to be a very well behaved model system for a detailed thermodynamic analysis *in vitro*, also because the ligand, tc, can be monitored easily via its particular fluorescence and absorption properties. In the present study we extend our structural insight from general features, like which parts of the RNA form the tc binding pocket, to details, such as the roles of particular nucleotides for interactions with the tc molecule or for the folding of the RNA structural core. We provide fundamental thermodynamic data that govern the interaction and that will help to understand the molecular and biochemical principles modulating the regulatory activity of aptamers. Finally, we also relate our *in vitro* data to observations *in vivo*, where frequently much higher ligand concentrations are necessary than indicated by the dissociation constants obtained from the pure molecules. Such information is invaluable for the construction of artificial riboswitches with different regulatory properties or novel ligand binding specificities.

MATERIALS AND METHODS

Preparation of aptamer RNA

The aptamers were transcribed *in vitro* from a linearized pSP64 plasmid (Promega) using a T7 promoter. For precise aptamer 3′ ends the primary transcripts contained self-cleaving hammerhead ribozymes (all sequences are available upon request). Run-off transcription was done in a volume of 2 ml containing 40 mM Tris-HCl (pH 8.0), 5 mM DTT, 1 mM spermidine, 30 mM Mg-acetate, 4 mM each NTP, 0.1 mg/ml HindIII-linearized plasmid and 15 μg/ml T7 RNA polymerase [prepared according (14)]. Reactions were incubated at 37°C for 4 h, subsequently diluted 1:5 in 30 mM Mg-acetate and subjected to two annealing cycles (5 min at 65°C, followed by slow-cooling to room temperature over 45 min) in order to maximize self cleavage of the ribozyme. After dissolving precipitated Mg-pyrophosphate by dropwise addition of 0.5 M EDTA (pH 8.0), the reaction products were pre-purified on 1 ml pre-equilibrated DEAE–Sepharose FF anion exchange resin [Pharmacia®, 0.7 cm column diameter, equilibration in 300 mM, elution in 3 M Na-acetate (pH 7.5)]. After ethanol-precipitation, the RNA products were separated on a 10% denaturing polyacrylamide gel. Aptamer RNA was detected by ultraviolet (UV) shadowing and eluted from crushed gel slices in 300 mM Na-acetate over night at room temperature. The supernatant was again concentrated on DEAE–Sepharose and ethanol precipitated. RNA was resuspended in H$_2$O (0.1–10 mg/ml) and stored frozen at −20°C. Prior to complex formation the RNA was adjusted to the respective buffer system and annealed (see above). Complexation with tc was assured by an additional co-incubation for 5 min at 37°C.

Analytical size exclusion chromatography

Analytical size exclusion chromatography was done on a Pharmacia SMART® system using a Superdex® 75 PC 3.2/30 column equilibrated at 25°C in binding buffer I [20 mM Tris-HCl (pH 7.5), 10 mM MgCl$_2$, 100 mM NaCl]. Stokes radii were determined using Pharmacia's low molecular weight calibration kit for gel filtration and the respective instructions. Typical starting concentrations of RNA were between 0.8 and 40 μM, with tc being 0 to 5 times that much. Injection volumes were 50 μl and flow rates typically at 70 μl/min. To keep both the RNA and tc absorption in the same measurable range, the optical extinction by the filtrate was monitored simultaneously at 290 nm (E$_{290}$) and at 374 nm (E$_{374}$), where tc has its absorption maximum. From these extinctions we estimated the concentrations of the individual components in the filtrate. To do so, the molar extinction coefficients ε$_{290}$ and ε$_{374}$ of both pure RNA (R) and pure tc (T) were obtained via Lambert–Beer's law from wavelength scans in binding buffer I of solutions with known concentrations. For this, the concentration of tc was determined experimentally according to (15), and the concentration of RNA was calculated from a value of 0.040 mg/ml for E$_{260}$ = 1 and from a molecular weight of 320 g/mol per nucleotide. Using Lambert–Beer's law, the concentration of RNA, c$_R$, in a mixture of RNA and tc can then be calculated as:

$$c_R = (E_{374} - E_{290} * \varepsilon_{T374}/\varepsilon_{T290})/[d * \varepsilon_{R290} * (\varepsilon_{R374}/\varepsilon_{R290} - \varepsilon_{T374}/\varepsilon_{T290})]$$

and the concentration of tc, c$_T$, accordingly as:

$$c_T = (E_{374} - E_{290} * \varepsilon_{R374}/\varepsilon_{R290})/[d * \varepsilon_{T290} * (\varepsilon_{T374}/\varepsilon_{T290} - \varepsilon_{R374}/\varepsilon_{R290})].$$

The pathlength d is in cm, concentrations are in mol/l and extinction coefficients are in l/(mol * cm). A potential hyperchromic effect on the absorption of tc upon binding to RNA was neglected.

Native polyacrylamide gel electrophoresis (PAGE)

Native gels (11 × 14 × 0.1 cm) were prepared in gel buffer [50 mM Tris-acetate (pH 7.5), 10 mM Mg-acetate] from 9.5% acrylamide and 0.5% N,N′-methylenebisacrylamide. They were run in gel buffer at 1 W for 6 h at room temperature, with a pre-run of 30 min. Samples (10 μl) contained 20 μM of RNA in binding buffer I. Tc was at 0 or 50 μM for the qualitative assays and within a range between those values for the titration. Just before loading 2.5 μl glycerol was added to a final concentration of 16% (v/v). After electrophoresis the gel was exposed immediately to UV light of 365 nm to visualize tc fluorescence. Then the RNA was stained for 10 min in a solution of ethidium bromide (1 μg/ml) and a second fluorescent image was taken. Densitometric quantification was done by the program TINA (Raytest, Straubenhardt, Germany) and a superposition of both images in false colors was done in Adobe Photoshop®.

Fluorescence titration spectroscopy (FTS)

The experiments were carried out at 25°C on a Fluorolog FL3–22. The excitation wavelength for all tc derivatives

was set at 370 nm [except for anhydro-tc (atc) at 455 nm]. The spectra were acquired from 450 nm to 600 nm in 1 nm increments with an integration time of 0.3 s. Slits were set to 2 mm. Tc or the tc derivative was presented in a nanomolar concentration in a total volume of 2 ml in binding buffer II [20 mM potassium phosphate buffer (pH 7.5), 100 mM NaCl, 10 mM MgCl$_2$]. The RNA was titrated in a way not to exceed a total volume increase of 5%. The solution was stirred during each titration step and allowed to equilibrate for 5 min before data collection. Fluorescence spectra were measured for each titration point. The peak area of the fluorescence emission signal was averaged, normalized and plotted against the free RNA concentration.

The fractional saturation (F$_S$) was determined by

$$F_S = (S - S_{min})/(S_{max} - S_{min}) = \Delta S/\Delta S_{max}$$

with ΔS as difference between fluorescence signal (S) and background fluorescence (S$_{min}$) at each particular titration step and ΔS_{max} as difference between the fluorescence maximum at complete saturation S$_{max}$ and S$_{min}$. The degree of saturation equals F$_S$ since the tc itself acts as acceptor molecule. The free RNA concentration was then calculated using

$$c_{freeRNA} = c_{totalRNA} - [F_S * c(tc)].$$

The saturation isotherm was fitted to the equation

$$F_S = [B_{max} * c_{freeRNA}/(K_d + c_{freeRNA})]$$

and results in the dissociation constant (K_d) and the maximum number of binding sites (B$_{max}$).

Isothermal titration calorimetry (ITC)

RNA and tc (or derivatives) were prepared in binding buffer I. Concentrations were determined by UV spectroscopy and were in the range of 0.8 to 6.0 µM for RNA and 9 to 50 µM for tc. ITC experiments were done on a MicroCal VP-ITC machine (MicroCal Inc. Northampton, MA) with the sample cell (1.44 ml) containing RNA. Following thermal equilibration at 25°C, an initial 60 s delay and an initial 2 µl injection, we typically did 24 serial injections of 10 µl or 19 serial injections of 15 µl tc at intervals of 180 s and at a stirring speed of 310 r.p.m. Raw data were recorded as power (µcal/s) over time (min). The heat associated with each titration peak was integrated and plotted against the respective molar ratio of tc and RNA and the resulting experimental binding isotherm was corrected for the effect of titrating tc into binding buffer I. Thermodynamic parameters were extracted from a curve fit to the corrected data using the one site binding model in the software (Origin 5.0) provided by MicroCal (MicroCal LLC). These are the change in enthalpy ΔH and the dissociation constant K_d. As a consequence, the change in Gibbs free energy ΔG and the change in entropy ΔS can be calculated from $\Delta G = -RT \ln(K_d)$ and $\Delta G = \Delta H - T\Delta S$, with T being the reaction temperature (in K) and R being the gas constant (1.986 cal K^{-1} mol^{-1}). For both fluorimetry and isothermal calorimetry the standard fitting errors from multiple measurements were combined, assuming a minimal error of 6% in determining final concentrations of ligand and RNA.

Green fluorescent protein (GFP) measurements

GFP measurements were done to analyze the ability of tc derivatives to regulate gene expression *in vivo*. We used a tc aptamer located in the 5′-UTR of a constitutively expressed *gfp* gene in yeast (11). For all experiments, *Saccharomyces cerevisiae* strain RS453α was transformed with plasmid pWHE601-AN32, which contains the tc-binding aptamer directly in front of the GFP start codon. pWHE601 which contains no aptamer was used as control for every measurement (11). Transformation was done according to the protocol supplied with the frozen EASY yeast transformation II kit (Zymo Research, Orange CA) and yeast cells were grown at 28°C for 48 h in minimal medium [0.7% (w/v) yeast nitrogen base, 2% (w/v) glucose, 12 µg/ml adenine, MEM amino acids, Gibco BRL] in the absence or presence of 100 µM of the respective tc derivatives in a final volume of 10 ml. Cells were harvested by centrifugation, washed twice in phosphate-buffered saline (PBS) and resuspended in 2 ml PBS. Each tc derivative was analyzed with three independently grown cultures. Fluorescence measurements were carried out at 25°C on a Fluorolog FL3–22, with the excitation wavelength set to 484 nm. The spectra were acquired from 490 to 530 nm in 1 nm increment with an integration time of 0.3 s. Slits were set to 2 mm. Additionally, we determined the OD at 600 nm to correlate the fluorescence intensity to the cell number. The relative GFP fluorescence was calculated with the fluorescence of pWHE601-AN32 in the absence of tc set to 100%. All measurements were repeated at least twice.

RESULTS AND DISCUSSION

The overall shape of the RNA remains constant upon tc-binding

Previous enzymatic and chemical probing experiments had shown that the two single-stranded parts B1-2 and L3 of the RNA aptamer molecule (Figure 1A) are affected by tc-binding and might come together to form a single binding pocket (13). In order to visualize potential changes of RNA conformation or multimerization state upon ligand binding we did analytical size exclusion chromatography experiments, in which we also monitored the migration behavior of tc at its peak absorption wavelength of 374 nm (Figure 2). Apo-RNA runs as a single sharp peak (Figure 2A, blue line) suggesting conformational homogeneity and the estimated Stokes radius of 26 Å indicates a monomer. In the presence of an excess of tc under saturating conditions neither the position nor the width of the RNA peak change significantly, while tc is clearly seen to be bound (Figure 2A, green and orange lines). This demonstrates that the RNA does not multimerize upon ligand binding and that there are no major conformational changes. The approximate concentrations of RNA and tc that were calculated from their respective extinction coefficients at 290 and 374 nm (see Materials and Methods) point to an equimolar tc–RNA complex (Figure 2B).

An identical series of experiments was done with a truncated version of the RNA aptamer, which we call minimer and which has the upper part of stem–loop 2 replaced by a
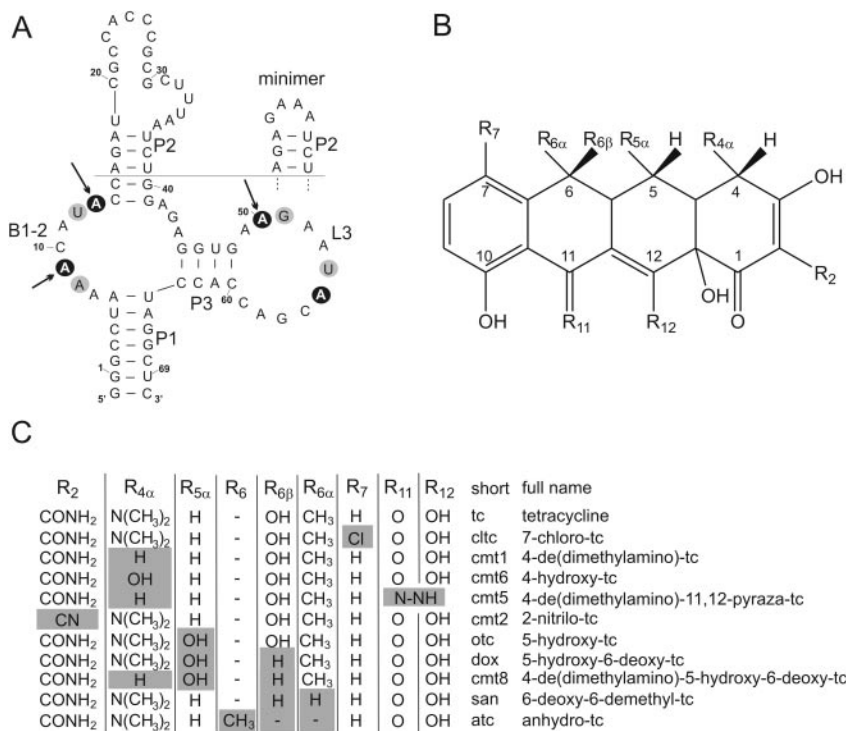
Figure 1. Secondary structure of the RNA aptamer and derivatives of tc. (**A**) The secondary structure of the tc aptamer as predicted by mFold (24) is supported by chemical and enzymatic probing (13). Important elements are indicated as stem = pedestal (P), bulge (B) and loop (L). Nucleotides analyzed by FTS are marked by grey circles. Nucleotides analyzed by both FTS and ITC are marked by black circles. Arrows indicate positions identified as important for tc-binding. The stem–loop 2 region of the minimer, where a GAAA tetraloop replaces nt 19–36 of the aptamer, is shown top right. (**B**) Structure of tc with positions mutated in this study denoted by R. (**C**) Chemical nomenclature of the derivatives and identity of the respective functional groups (cmt = chemically modified tc).
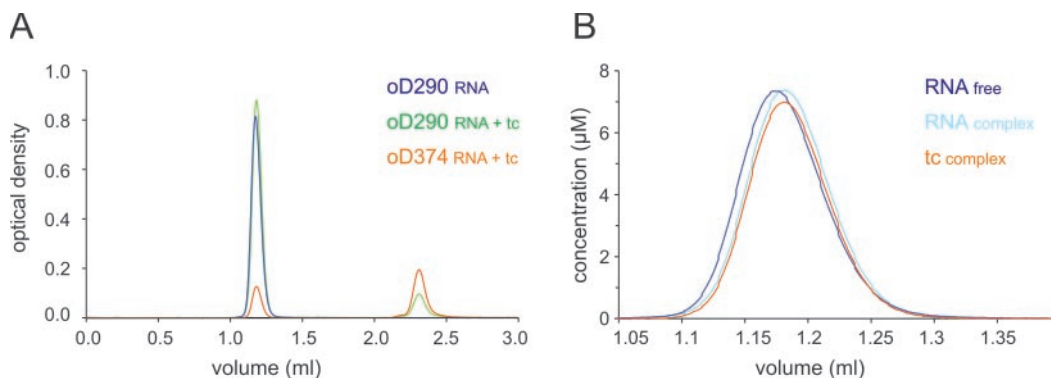

Figure 2. Analytical size exclusion chromatography. (**A**) Superimposed chromatograms of 1 nmol free RNA (blue) and of 1 nmol RNA in the presence of 3 nmol tc (green and orange). Injection volumes were 50 µl and optical densities were monitored at 290 nm (blue or green) and 374 nm (orange), where tc is detected exclusively. Excessive tc elutes at 2.32 ml. (**B**) Quantification of RNA (cyan or blue) and tc (orange). An equimolar stoichiometry is observed in the tc–RNA complex from (A). The elution volume of the RNA of 1.18 ml (Stokes radius 26 Å) indicates a monomer. No major conformational changes can be detected between free and complexed RNA.

stabilizing GAAA-tetraloop (Figure 1A, top right). Apart from a later elution from the size exclusion column due to its smaller size (Stokes radius 24 Å) the minimer behaves very similarly to the full-length aptamer (data not shown). This confirms and supports our previous interpretation of probing data, where we suspected the upper part of stem–loop 2 to be dispensable for tc-binding (13).

The behavior of the minimer was also analyzed by native PAGE since this method is frequently more sensitive to conformational changes than size exclusion chromatography (Figure 3). RNA was pre-incubated with increasing amounts of ligand and applied to the gel. After electrophoresis, tc was detected via its characteristic fluorescence caused by excitation with UV light of 365 nm. Ethidium bromide-stained RNA was visualized subsequently. Co-localization of RNA and tc was demonstrated by the superposition of both images in false colors. The minimer RNA does not change its migration behavior upon ligand binding (Figure 3A). Densitometric
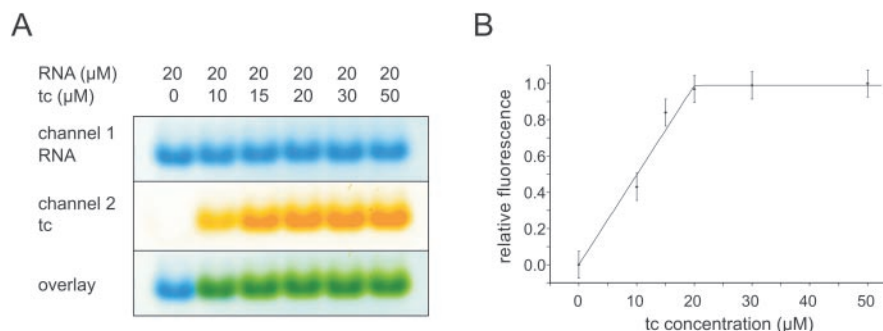
Figure 3. Native PAGE. (**A**) Visualization of tc-binding (false colors). RNA (20 µM of the minimer variant) was incubated with increasing amounts of tc and applied to a 10% polyacrylamide gel. Tc was visualized directly by fluorescence (middle panel), RNA subsequently via staining with ethidium bromide (upper panel). Co-localization is demonstrated by the overlay (lower panel). No major conformational changes can be detected between free and complexed RNA. (**B**) Densitometric quantification. Saturation at 20 µM tc supports an equimolar stoichiometry.

quantification of the titration experiment shows again an equimolar stoichiometry (Figure 3B).

In summary, the demonstration of a conformationally homogeneous 1:1 complex of RNA and tc under saturating conditions high above the dissociation constant K_d (see below) justifies the previous interpretation of enzymatic and chemical probing data, where this stoichiometry had always been assumed. It also makes the system ideally suited for a further biophysical analysis.

The interaction of aptamer RNA with tc is exceptionally strong

The size exclusion chromatography and native PAGE assays indicated an exceptional thermodynamic stability of the complex. Therefore, we decided to use FTS to characterize the thermodynamic properties of the interaction of tc with the full-length RNA aptamer. This method exploits the increase in tc fluorescence when the molecule passes from an aqueous environment in solution to a more hydrophobic environment in the RNA complex. It delivers accurate dissociation constants even in the sub-nanomolar range (Figure 4).

We titrated tc (0.5 nM) with increasing amounts of RNA and plotted the fractional saturation of tc as a function of the concentration of free RNA. Applying a single binding site model we obtain a dissociation constant K_d of 770 pM at half saturation (Figure 4B). This is about three orders of magnitude lower than assumed previously and corresponds to a standard free energy ΔG of −12.43 kcal/mol (Table 1). Such a tight binding is unusual for a small ligand like tc and points to multiple stacking and bonding interactions with the RNA. Among small molecule RNA aptamers the present dissociation constant is the lowest reported.

Magnesium ions are essential for binding. When divalent ions are absent from the titration experiment (in the presence of 1 mM EDTA), only marginal tc-binding is detected. Addition of magnesium chloride to a final concentration of 15 mM, however, restores previous tc fluorescence levels. It is well possible that in addition to its usual function in RNA tertiary structure formation (16), Mg^{2+} assists tc-binding directly in a composite site at the RNA-tc interface. Tc chelates Mg^{2+} via its ketoenol group (17) and a tc-dependent Mg^{2+} site has been detected in the vicinity of nucleotide A55 (13).

## Base substitutions that lower tc affinity reduce the efficiency of the riboswitch *in vivo*

For a more detailed understanding of the roles of individual nucleotides for RNA structure, tc-binding and *in vivo* regulation we selected interesting positions within the RNA aptamer for a mutational analysis. Among those that show the most direct tc-dependent protection from chemical probing (A09$^{N7\&N1}$, U12^{N3}, A13$^{N7>N1}$, A49$^{N7>N1}$, A50$^{N7>N1}$, G51$^{N1\&N2}$, U54^{N3}, A55^{X}, G57$^{N1\&N2}$) we selected three positions (A09, A13, A50) that are intolerant and three positions (G51, U54, A55) that are tolerant to mutation with respect to tc-dependent regulation of translation *in vivo* (13). As an additional control, we included A08, which gets only marginally protected by tc at its nitrogen N7 and tolerates mutation with respect to regulation rather well. The positions U54 and A55 were also chosen because of their proximity to the RNA backbone site that becomes hypersensitive to hydroxyl radical cleavage in the presence of tc (13).

FTS shows the affinities for tc of the A09G, A13U and A50U mutants to be significantly reduced, about 200- to 300-fold. The mutants G51U, U54G and A55G have an only 2- to 4-fold reduced affinity, whereas the affinity of the A08G control is almost unchanged (Table 1). Pairwise and overall comparisons show that the ability of the RNA to bind tc and the ability to regulate translation *in vivo* correlate well (Table 1).

Apparently, the identities of nucleotides A08, G51, U54 and A55 are only of secondary importance for tc-binding and regulatory activity. Nevertheless, residues in loop L3 might still contact the ligand via backbone or stacking interactions and induce local changes of RNA conformation. This would explain why the RNA backbone gets resistant to cleavage by the single strand-specific nuclease S1 and hypersensitive to hydroxyl radicals and why some functional groups on the bases are no longer accessible to chemical probes (13).

The hydroxyl at tc position $R_{6\beta}$ is highly important for RNA binding and riboswitch activity

Tc is a flat polycyclic molecule with four fused rings carrying hydrophilic functional groups and one aromatic ring (Figure 1B). Thus, one face of the molecule is able to make ionic interactions, while the other face allows either hydrophobic or stacking interactions. We analyzed a series
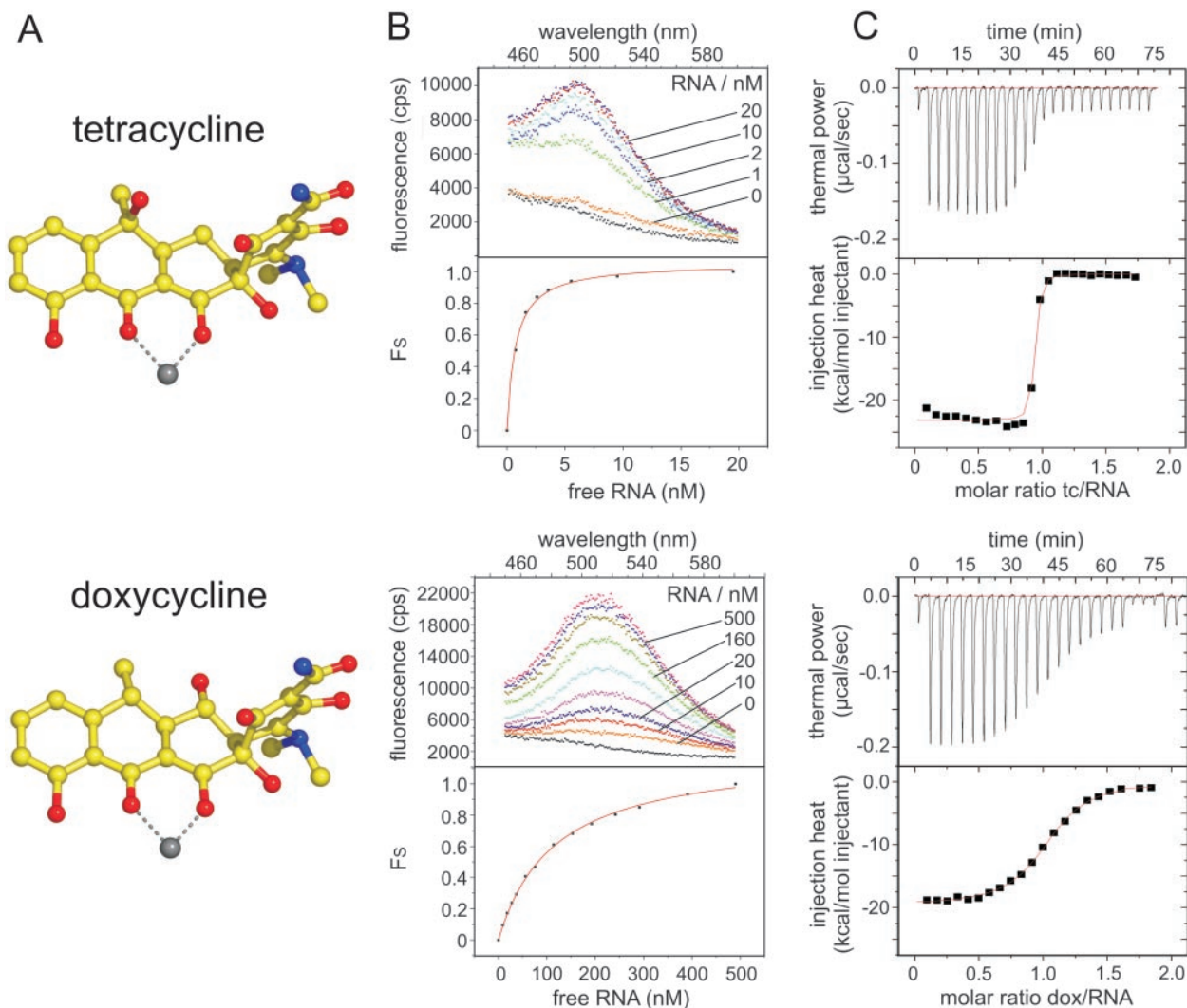
Figure 4. Determination of equilibrium dissociation constants (K_d) by FTS and ITC. (**A**) 3D structures of tc and dox as ball-and-stick models, respectively, (carbons: yellow, oxygens: red, nitrogens: blue, magnesium ion: grey). (**B**) FTS. Upper panels: fluorescence spectra of constant amounts of tc (0.5 nM) and dox (10 nM), respectively, that were titrated with increasing amounts of RNA until saturation was reached (black lines: spectra of buffer). Lower panels: the fractional saturation of the ligand (Fs) plotted against the concentration of free RNA and fitted to a single binding site model. (**C**) ITC. Upper panels: power required to maintain the temperature of the RNA solution (tc: 1.7 µM, dox: 2.6 µM; 1.44 ml) recorded over the time of multiple injections (10 µl) of ligand (tc: 23 µM, dox: 36 µM) until saturation was reached (baseline-corrected). Lower panels: integrated heats of interaction plotted against the molar ratio of ligand over RNA and fitted to a single binding site model.

of tc derivatives (Figure 1C) with single or multiple sub-stitutions of functional groups. This does not only provide information on the substrate specificity of the RNA aptamer, but also generates insight into the relative orientation of tc with respect to the RNA in the complex.

Dissociation constants were determined by FTS and are listed in Table 2. The addition of a chlorine group at position R_7 (7-chloro tc, cltc) or of a hydroxyl group at position $R_{5\alpha}$ (5-hydroxy-tc, otc) does not significantly disturb the interaction. The replacement of the dimethylamino group at position $R_{4\alpha}$ either by a hydroxyl group (cmt6) or a simple hydrogen (cmt1) causes only a small drop in binding energy. In the context of cmt1 the additional exchange of the ketoenolate at position R_{11}–R_{12} by a pyraza group (cmt5) is even slightly favorable, possibly because it rigidifies the ligand even

more. Position R_2 is much more crucial, since the replacement of the amide group with cyanide (cmt2) reduces binding more than 10-fold. The most dramatic effect, a more than 100-fold reduction of binding, is obtained by the removal of the hydroxyl group at position $R_{6\beta}$. This is obvious from the comparison of doxycycline (dox) with otc and from the comparison of cmt8 with otc and cmt1. In sancycline (san) and anhydro-tc (atc) this effect is present as well, albeit masked by apparently compensating rearrangements. These might be due to an sp²-hybridized carbon C6, which generates an increased stacking surface (Figure 1B, Table 2). Lower affinities again result in lower regulation efficiencies of the riboswitch *in vivo*, although the analysis is complicated in this case by different degrees of membrane permeability and toxicity of the respective tc derivatives.

Table 1. Thermodynamic values of tc binding to aptamer mutants and the respective efficiencies of regulation

RNA	FTS K_d nM	ΔG kcal/mol	$\Delta\Delta G$ kcal/mol	ITC K_d nM	ΔG kcal/mol	$\Delta\Delta G$ kcal/mol	ΔH kcal/mol	$-T\Delta S$ kcal/mol	$\Delta\Delta H$ kcal/mol	$-T\Delta S$ kcal/mol	$\Delta(-T\Delta S)$ kcal/mol	Regulation[a] In vivo
wt	0.77 ± 0.11	−12.428 ± 0.087		see FTS	see FTS		−22.9 ± 1.5	10.5 ± 1.5				5.8
A08G	1.05 ± 0.12	−12.252 ± 0.068	0.18 ± 0.11									3.1
A09G	162 ± 16	−9.263 ± 0.059	3.16 ± 0.11	402 ± 69	−8.73 ± 0.10	3.70 ± 0.13	−28.4 ± 2.6	19.7 ± 2.6	−5.50 ± 3.0	9.2 ± 3.0		1.0
A13U	222 ± 22	−9.077 ± 0.058	3.35 ± 0.10	189 ± 18	−9.174 ± 0.056	3.25 ± 0.10	−20.1 ± 1.1	11.0 ± 1.1	2.8 ± 1.9	0.6 ± 1.9		0.9
A50U	196 ± 24	−9.152 ± 0.071	3.28 ± 0.11	208 ± 12	−9.117 ± 0.035	3.311 ± 0.094	−10.12 ± 0.64	1.00 ± 0.65	12.8 ± 1.7	−9.5 ± 1.7		0.9, 0.9[b]
G51U	2.93 ± 0.19	−11.641 ± 0.039	0.786 ± 0.095									3.0
U54G	2.63 ± 0.23	−11.704 ± 0.052	0.72 ± 0.10									3.3
A55G	1.69 ± 0.35	−11.97 ± 0.12	0.46 ± 0.15	7.19 ± 0.66	−11.109 ± 0.054	1.32 ± 0.10	−21.8 ± 1.3	10.6 ± 1.3	1.2 ± 2.0	0.2 ± 2.0		2.9[c]

[a]The efficiency of regulation *in vivo* is given as the ratio of GFP fluorescence without and with 100 μM tc in the medium. A control construct without an aptamer sequence in the 5′-UTR [pWHE601, (11)] was tested in parallel and showed no tc-dependent decrease in GFP fluorescence.
[b]A50U is not measurable due to the introduction of a premature start codon. The values were determined for A50G and A50C, respectively.
[c]A55G was measured as double mutant in combination with U53C to prevent the formation of a premature start codon.

The hydroxyl at tc position $R_{6\beta}$ interacts with nucleotide A13 of aptamer RNA

In an attempt to identify interactions of defined functional groups of tc with individual nucleotides of RNA we determined dissociation constants of selected RNA point mutants with a number of tc derivatives (Table 2). In this variation of a double mutant cycle analysis (18) we first determine the difference in binding energy between an interaction of an RNA point mutant with a tc derivative as compared to the interaction of wt RNA with tc ($\Delta\Delta G_{TR}$). Then we determine the loss of binding energy resulting from each individual mutation separately ($\Delta\Delta G_T$ and $\Delta\Delta G_R$). If the sum of $\Delta\Delta G_T$ and $\Delta\Delta G_R$ equals $\Delta\Delta G_{TR}$ this indicates that both mutations affect different interactions. If the sum of the $\Delta\Delta G_T$ and $\Delta\Delta G_R$ is larger than $\Delta\Delta G_{TR}$ this indicates that both mutations affect a common interaction (Figure 5).

We analyzed the addition of a hydroxyl group on tc at position $R_{5\alpha}$ (otc versus tc), the removal of the hydroxyl group at position $R_{6\beta}$ (dox versus otc) and the exchange of the amide group at position R_2 against cyanide (tc versus cmt2) in the context of the three relevant RNA point mutants A09G, A13U and A50U. As shown in Table 3 and Figure 5B the most obvious interaction is between nucleotide A13 and the hydroxyl group at position $R_{6\beta}$ of tc with a free energy of interaction, $\Delta\Delta G_{int}$, that amounts to −1.59 kcal/mol. This accounts for >50% of the effect of each single mutation ($\Delta\Delta G_T$ or $\Delta\Delta G_R$) indicating the interaction between A13 and the $R_{6\beta}$ hydroxyl to be the major one for each of the two participating groups. The interaction of the aptamer with the $R_{6\beta}$ hydroxyl group might also be slightly affected by the A50U mutation, but the major effect of both the A50U and A09G mutations are additive to the effect of the changes on tc. Therefore, it is well possible that the major contributions of these two nucleotides to tc-binding result from stacking interactions and/or from their roles in pre-structuring the RNA for ligand binding.

An unfavorable entropy of tc-binding indicates local RNA folding and ion fixation

ITC is an alternative and complementary method to FTS. It delivers very accurate dissociation constants by measuring the heat of complexation at each step of the titration process (Figure 4). This not only provides the free energy of complexation (ΔG), but uniquely allows distinguishing between the enthalpic (ΔH) and entropic ($-T\Delta S$) contributions of the process. In round terms, the enthalpic contributions are correlated with the making and breaking of molecular interactions, whereas the entropic contributions are correlated with the change of order in the system that includes both macromolecules and solvent. This provides additional insight into the mode of ligand binding. The drawback of ITC is its slightly lower sensitivity (down to the low nanomolar range) and the considerable amount of RNA that is consumed in each titration.

ITC gave an estimate of the dissociation constant, K_d, of 660 pM ($\Delta G = -12.52$ kcal/mol). The detection limits of the instrument made us compromise for a very steep transition of the titration curve (Figure 4C) with only few data points, but the obtained value for the free binding energy, ΔG, is in good agreement with the one obtained from FTS

Table 2. Binding constants of tc derivatives and the respective efficiencies of regulation

Derivative Abbreviation	Chemical designation	FTS	K_d nM	ΔG kcal/mol	$\Delta\Delta G$ kcal/mol	Regulation[a] *In vivo*
tc	tc	wt	0.77 ± 0.11	−12.428 ± 0.087		5.8
cltc	7-chloro-tc	wt	0.573 ± 0.092	−12.608 ± 0.096	−0.18 ± 0.13	3.8
cmt1	4-de (dimethyamino)-tc	wt	1.97 ± 0.89	−11.88 ± 0.27	0.55 ± 0.28	1.4[b]
cmt6	4-hydroxy-tc	wt	2.77 ± 0.44	−11.674 ± 0.093	0.75 ± 0.13	2.0
cmt5	4-de (dimethyamino)-11,12-pyraza-tc	wt	0.46 ± 0.99	−12.8 ± 1.3	−0.3 ± 1.3	2.0
cmt2	2-nitrilo-tc	wt	9.8 ± 1.1	−10.926 ± 0.067	1.50 ± 0.11	1.3
otc	5-hydroxy-tc	wt	1.78 ± 0.32	−11.94 ± 0.10	0.49 ± 0.14	4.5
dox	5-hydroxy-6-deoxy-tc (doxycycline)	wt	118 ± 12	−9.453 ± 0.060	2.97 ± 0.11	1.1
cmt8	4-de (dimethyamino)-5-hydroxy-6-deoxy-tc	wt	547 ± 47	−8.543 ± 0.051	3.89 ± 0.10	nd[c]
san	6-deoxy-6-demethyl-tc (sancycline)	wt	22.2 ± 4.8	−10.44 ± 0.13	1.99 ± 0.16	1.3
atc	anhydro-tc	wt	3.5 ± 2.6	−11.53 ± 0.44	0.90 ± 0.45	nd[c]
otc		A9G	445 ± 28	−8.665 ± 0.037	3.763 ± 0.095	
cmt2		A9G	2640 ± 190	−7.611 ± 0.043	4.817 ± 0.097	
dox		A9G	17 700 ± 4400	−6.48 ± 0.15	5.94 ± 0.17	
otc		A13U	532 ± 94	−8.56 ± 0.10	3.87 ± 0.14	
cmt2		A13U	1700 ± 160	−7.870 ± 0.055	4.56 ± 0.10	
dox		A13U	2420 ± 190	−7.661 ± 0.045	4.767 ± 0.098	
otc		A50U	600 ± 40	−8.483 ± 0.039	3.944 ± 0.095	
cmt2		A50U	2570 ± 170	−7.626 ± 0.039	4.802 ± 0.095	
dox		A50U	10500 ± 2600	−6.79 ± 0.15	5.64 ± 0.17	

[a]The efficiency of regulation *in vivo* is given as the ratio of GFP fluorescence without and with 100 µM tc in the medium. A control construct without an aptamer sequence in the 5′-UTR [pWHE601, (11)] was tested in parallel and showed no tc-dependent decrease in GFP fluorescence.
[b]The regulation *in vivo* was determined in presence of only 20 µM cmt1, due to growth inhibition at higher concentrations.
[c]The regulation *in vivo* was not detectable due to growth inhibition caused by the respective tc derivative.

(Table 1). The free binding enthalpy, ΔH, which still can be measured much more reliably under such experimental conditions (19) was determined at −22.9 kcal/mol. Using the well-determined free binding energy from fluorimetry, this results in an unfavorable entropic contribution, $-T\Delta S$, of +10.5 kcal/mol (Table 1, Figure 6). The enormously favorable binding enthalpy can be attributed not only to the formation of inter-molecular bonds and stacking interactions between tc and the RNA, but also to tc-induced intramolecular interactions within the RNA aptamer and ion fixation. The considerably unfavorable entropy might arise from complexation itself, but certainly also from the loss of flexibility resulting from local RNA folding. Such local effects do not necessarily change the overall shape of the molecule and are hence not detectable by size exclusion chromatography or native PAGE. Very importantly, the entropic term is also affected by solvent effects like the additional fixation of magnesium ions. As with FTS we noticed a crucial role of magnesium ion for complex formation by monitoring the free binding enthalpy in separate experiments, albeit without detailed quantification.

Two-step binding of tc may involve an induced fit of RNA loop L3

Mutations at the crucial positions A09, A13 and A50 still result in affinities for tc that are in the sub-micromolar range. This made them suitable for an in-depth analysis by ITC (Figure 6). The free binding energies (ΔG) obtained for tc with the A09G, A13U, A50U and A55G mutants agree well with the ones obtained by FTS (Table 1, Figure 6A). Again, the identity of the base at position A55 is of little importance and both enthalpic and entropic contributions to tc-binding change only marginally with respect to wild-type (wt) RNA. For the other three mutants, despite

comparable losses in free binding energy with respect to wt, the relative enthalpic and entropic contributions to this effect vary dramatically (Figure 6B). In the case of A13U the loss of tc affinity is mainly due to a reduced binding enthalpy and in the case of A09G it is the entropic term, which is considerably more unfavorable than in the wt. For A50U there is an enormous loss in binding enthalpy, which is compensated by the complete disappearance of the unfavorable entropic term.

Because the double mutant cycle analysis had indicated an interaction of A13 with the hydroxyl group at position $R_{6\beta}$ of tc, we also did an experiment with wt RNA and dox (Figures 4 and 6). As in the case of the A13U mutation, the loss of affinity associated with the removal of the hydroxyl group is almost exclusively enthalpic. This points to a first, rigid body contact between the RNA and tc at these positions that on its own does not induce any major refolding. Together with the small size of a hydroxyl group this observation supports the idea that the interaction identified by the double mutant cycle analysis is a direct one.

The adenine A09 could be important for pre-structuring the RNA, possibly with an interaction that is broken upon ligand binding. In the A09G mutation this structure would be absent and would have to be induced by tc-binding, increasing the entropic penalty. This interpretation is supported by facilitated translation *in vivo* of A09 point mutants (13).

In the case of the A50U mutation, a whole series of—entropically costly—tc-RNA or RNA-RNA interactions seems to be prevented. We therefore favor a scenario in which a possible interaction of A50 with tc (stacking?) triggers parts of loop L3 to fold appropriately. This second step of binding might bring the adjacent nucleotide G51 into position for being crosslinked to tc (20) and might also create the tc-dependent Mg^{2+}-site near the backbone of nucleotide A55 (13).

Table 3. Double mutant cycle analysis and energies of interaction

	$\Delta\Delta G_T$ kcal/mol	$\Delta\Delta G_R$ kcal/mol	$\Delta\Delta G_{TR}$ kcal/mol	$\Delta\Delta G_{int}$ kcal/mol[a]
wt–A09G				
tc–otc	0.49 ± 0.14	3.16 ± 0.11	3.763 ± 0.095	0.11 ± 0.15
tc–cmt2	1.50 ± 0.11	3.16 ± 0.11	4.817 ± 0.097	0.15 ± 0.13
otc–dox	2.48 ± 0.12	3.27 ± 0.11	5.45 ± 0.18	−0.30 ± 0.19
otc–cmt2	1.01 ± 0.12	3.27 ± 0.11	4.33 ± 0.11	0.04 ± 0.14
tc–dox	2.97 ± 0.11	3.16 ± 0.11	5.94 ± 0.17	−0.19 ± 0.19
cmt2–dox	1.473 ± 0.090	3.315 ± 0.079	4.44 ± 0.16	−0.34 ± 0.18
wt–A13U				
tc–otc	0.49 ± 0.14	3.35 ± 0.10	3.87 ± 0.14	0.03 ± 0.18
tc–cmt2	1.50 ± 0.11	3.35 ± 0.10	4.56 ± 0.10	−0.29 ± 0.14
otc–dox	2.48 ± 0.12	3.38 ± 0.15	4.28 ± 0.11	−1.59 ± 0.17
otc–cmt2	1.01 ± 0.12	3.38 ± 0.15	4.07 ± 0.12	−0.32 ± 0.17
tc–dox	2.97 ± 0.11	3.35 ± 0.10	4.767 ± 0.098	−1.56 ± 0.13
cmt2–dox	1.473 ± 0.090	3.056 ± 0.086	3.265 ± 0.081	−1.26 ± 0.11
wt–A50U				
tc–otc	0.49 ± 0.14	3.28 ± 0.11	3.944 ± 0.095	0.18 ± 0.16
tc–cmt2	1.50 ± 0.11	3.28 ± 0.11	4.802 ± 0.095	0.02 ± 0.14
otc–dox	2.48 ± 0.12	3.45 ± 0.11	5.14 ± 0.18	−0.79 ± 0.19
otc–cmt2	1.01 ± 0.12	3.45 ± 0.11	4.31 ± 0.11	−0.15 ± 0.14
tc–dox	2.97 ± 0.11	3.28 ± 0.11	5.64 ± 0.17	−0.61 ± 0.19
cmt2–dox	1.473 ± 0.090	3.300 ± 0.077	4.13 ± 0.16	−0.64 ± 0.18

[a]$\Delta\Delta G_{int} = \Delta\Delta G_{TR} - (\Delta\Delta G_T + \Delta\Delta G_R)$.
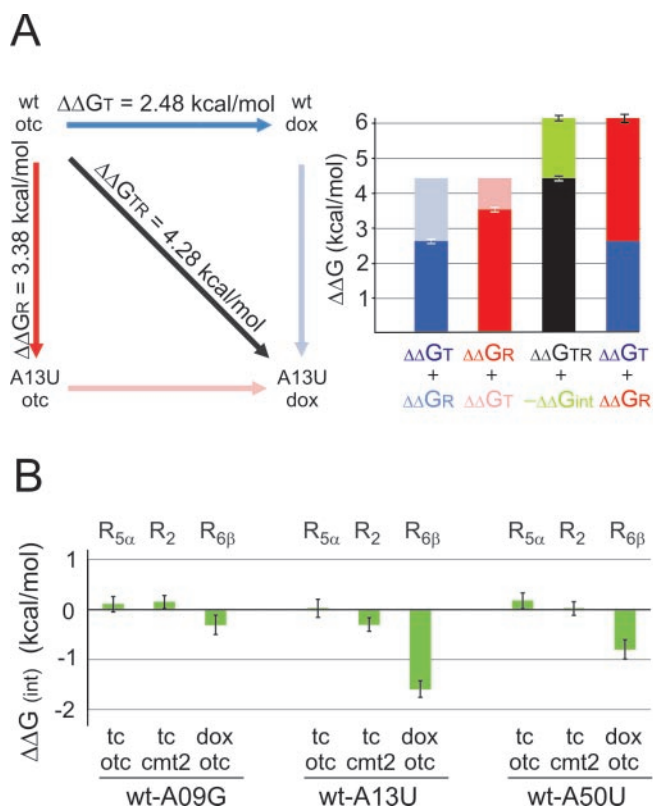
**Figure 5.** Double mutant cycle analysis. Gibbs free energies of interaction and the respective difference values ($\Delta\Delta G$) were determined by FTS for various combinations of RNA mutants and tc derivatives. Two functional groups interact favorably, if the effect of the double mutant ($\Delta\Delta G_{TR}$) is less than the sum of the effects ($\Delta\Delta G_T + \Delta\Delta G_R$) of the single mutants [$\Delta\Delta G_{int} < 0$; $\Delta\Delta G_{int} = \Delta\Delta G_{TR} - (\Delta\Delta G_T + \Delta\Delta G_R)$]. (**A**) Representative analysis, shown for the interaction of the hydroxyl group at position $R_{6\beta}$ of tc and nucleotide A13. (**B**) $\Delta\Delta G_{int}$ values for the indicated positions of tc, calculated from the respective combination of RNA- and tc-variants. The most obvious interaction is between the hydroxyl group at position $R_{6\beta}$ of tc and nucleotide A13.

The importance of a correctly folded loop L3 for tc-binding is also demonstrated by the behavior of a previously characterized RNA variant, A55U (13), in the native PAGE assay (Figure 7). The presence of this point mutation in the molecular context of either the RNA aptamer or the minimer leads to a second band with lower electrophoretic mobility that probably results from the dimerization of the RNA via loop L3. The A55U nucleotide exchange results in a palindromic L3 sequence GAAUUC that allows the formation of a kissing loop dimer. Tc migrates only with the monomeric form. Whereas the identity of the nucleotide at position 55 as such seems to be of little importance for ligand binding [see Table 1, (13)], its orientation and/or the conformation of the affected loop L3 seems to be of particular importance, e.g. for a direct or ion-mediated contact to tc.

CONCLUSION

The observed dissociation constant of 770 pM is exceptional for the interaction of an RNA with a small molecule ligand. Comparable targets that are either bound by *in vitro* selected RNA aptamers or by naturally occurring riboswitches usually have an affinity that is lower by at least one to two orders of magnitude. The only examples of even stronger complexes are with bigger targets, such as proteins that provide a much larger number of functional groups for possible interactions. More ancient versions of the aptamer, based on the cb28 variant (20), had indicated dissociation constants of only around 100 nM. The more than 100-fold better binding in the present case might be due to the absence of extensive overhangs at the 5′ and 3′ ends and due to a better pre-structuring of the molecule. In order to explain the exceptional affinity of the tc riboregulator one has to assume that the functional groups and stacking surfaces of tc are exploited to a much higher degree than, for example, in the complexes with ribosomal RNA (21,22), where the affinities are worse than 1 μM (23).
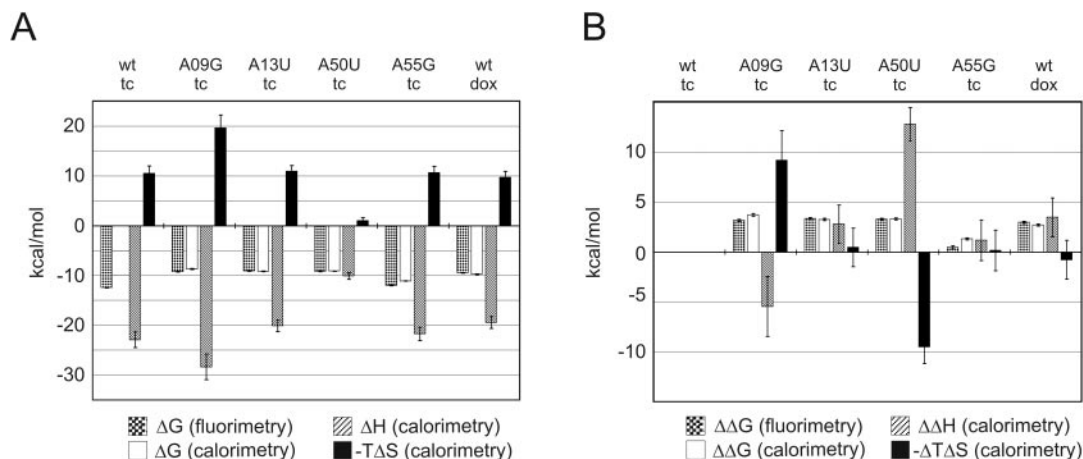
Figure 6. ITC of variants of RNA and tc. (**A**) Gibbs free energies (ΔG), enthalpic (ΔH) and entropic contributions ($-T\Delta S$). Values for ΔG obtained by FTS and ITC agree well. (**B**) Difference values for Gibbs free energy ($\Delta\Delta G$), enthalpy ($\Delta\Delta H$) and the entropic term ($-\Delta T\Delta S$). Values were calculated with respect to wt RNA and tc. Enthalpic (ΔH) and entropic contributions ($-T\Delta S$) obtained by ITC vary significantly for the respective molecular variants.
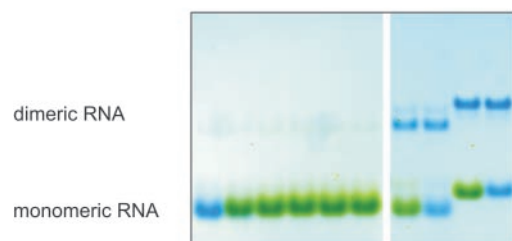
Figure 7. Native PAGE of an RNA loop L3 mutant (A55U). RNA (20 μM) was incubated with up to 50 μM tc and applied to a 10% polyacrylamide gel (see Figure 3 for details). Left side: titration of wt minimer RNA used for quantification in Figure 3. Right side: A55U mutants in the context of minimer and aptamer RNA. The slower migrating band probably represents RNA dimers that can form via L3 kissing loops. Tc preferentially runs with the monomer, indicating the importance of loop L3 conformation for ligand binding.

Our analysis leads to a picture of the RNA–tc complex, where the functional groups on one side of tc are read out by direct contacts to the RNA. The respective surface of tc includes in close proximity the important $R_{6\beta}$ hydroxyl group, the R_2 amide group and the oxygen at carbon C1, which was not included in our analysis. The $R_{6\beta}$ hydroxyl group interacts with nucleotide A13, where the nitrogen N7 might play a particularly important role, because it gets protected from chemical modification only in the presence of tc (13). The aromatic part of tc is available for stacking interactions with nucleotide bases like A50. A09 seems to be mostly important for pre-structuring the apo-RNA. Finally, the ketoenolate of tc could chelate a magnesium ion that might contact the phosphoribose backbone of loop L3 close to position 55 (13), further stabilizing the complex.

Gel filtration and native PAGE in the presence of Mg^{2+} detect no major conformational changes between the apo- and tc-bound states of the RNA. Tc therefore rather seems to stabilize an already pre-existing structure. However, this does not preclude local RNA folding, which can lead to additional intramolecular contacts and ion fixation as indicated by the very unfavorable binding entropy. ITC of RNA and tc variants and previously published probing data (13) are consistent with tc-binding in two steps: an initial rigid body docking via the A13-$R_{6\beta}$ interaction followed by an induced folding of loop L3. The resulting pseudoknot-like structure with possible contacts between loop L3 and bulge B1–2 can explain the regulatory properties of the RNA: while the scanning ribosome might be able to melt the stem–loops of the apo-structure in a zipper-like fashion, the stabilized pseudoknot might present a much stronger obstacle (12).

Despite the exceptional affinity for tc *in vitro* the present RNA regulator requires ligand concentrations for applications *in vivo* that are 100- to 1000-fold higher than indicated by the dissociation constant. This discrepancy is similar to other engineered systems (6) and currently the biggest obstacle for the development of highly sensitive riboregulators in higher eukaryotes. The reasons for this are poorly understood. Certainly, ionic conditions and alternative RNA conformations in the cell, competition with the binding of proteins and other RNAs and the dynamics of the competing processes play an important role (12). The effects of RNA mutations, however, are relevant *in vivo* and do correlate with the observations *in vitro*. The present thermodynamic analysis therefore provides the tools and fundamental data for improving the regulatory properties of the tc riboregulator in a rational way (e.g. by destabilizing the apo-structure) and we expect that similar techniques can be applied to the ligand binding domains of more complex, also naturally occurring riboswitches. It will therefore be interesting to see how the predictions for the present, well-studied model complex are matched by a detailed 3D structure that we are seeking to obtain.

Conflict of interest Statement. None declared.

REFERENCES

1. Winkler,W.C. and Breaker,R.R. (2003) Genetic control by metabolite-binding riboswitches. *Chembiochem.*, **4**, 1024–1032.
2. Mandal,M. and Breaker,R.R. (2004) Gene regulation by riboswitches. *Nature Rev. Mol. Cell. Biol.*, **5**, 451–463.
3. Tucker,B.J. and Breaker,R.R. (2005) Riboswitches as versatile gene control elements. *Curr. Opin. Struct. Biol.*, **15**, 342–348.
4. Winkler,W.C. and Breaker,R.R. (2005) Regulation of bacterial gene expression by riboswitches. *Ann. Rev. Microbiol.*, **59**, 487–517.
5. Suess,B. (2005) Engineered riboswitches control gene expression by small molecules. *Biochem. Soc. Trans.*, **33**, 474–476.
6. Bauer,G. and Suess,B. (2006) Engineered riboswitches as novel tools in molecular biology. *J. Biotechnol.*, epub ahead.
7. Hermann,T. and Patel,D.J. (2000) Adaptive recognition by nucleic acid aptamers. *Science*, **287**, 820–825.
8. Patel,D.J., Suri,A.K., Jiang,F., Jiang,L., Fan,P., Kumar,R.A. and Nonin,S. (1997) Structure, recognition and adaptive binding in RNA aptamer complexes. *J. Mol. Biol.*, **272**, 645–664.
9. Werstuck,G. and Green,M.R. (1998) Controlling gene expression in living cells through small molecule-RNA interactions. *Science*, **282**, 296–298.
10. Harvey,I., Garneau,P. and Pelletier,J. (2002) Inhibition of translation by RNA-small molecule interactions. *RNA*, **8**, 452–463.
11. Suess,B., Hanson,S., Berens,C., Fink,B., Schroeder,R. and Hillen,W. (2003) Conditional gene expression by controlling translation with tetracycline-binding aptamers. *Nucleic Acids Res.*, **31**, 1853–1858.
12. Hanson,S., Berthelot,K., Fink,B., McCarthy,J.E.G. and Suess,B. (2003) Tetracycline-aptamer-mediated translational regulation in yeast. *Mol. Microbiol.*, **49**, 1627–1637.
13. Hanson,S., Bauer,G., Fink,B. and Suess,B. (2005) Molecular analysis of a synthetic tetracycline-binding riboswitch. *RNA*, **11**, 503–511.
14. Davanloo,P., Rosenberg,A.H., Dunn,J.J. and Studier,F.W. (1984) Cloning and expression of the gene for bacteriophage T7 RNA polymerase. *Proc. Natl Acad. Sci. USA*, **81**, 2035–2039.
15. Sigler,A., Schubert,P., Hillen,W. and Niederweis,M. (2000) Permeation of tetracyclines through membranes of liposomes and *Escherichia coli*. *Eur. J. Biochem.*, **267**, 527–534.
16. Yamauchi,T., Miyoshi,D., Kubodera,T., Nishimura,A., Nakai,S. and Sugimoto,N. (2005) Roles of Mg2+ in TPP-dependent riboswitch. *FEBS Lett.*, **579**, 2583–2588.
17. Schmitt,M.O. and Schneider,S. (2000) Spectroscopic investigation of complexation between various tetracyclines and Mg^{2+} or Ca^{2+}. *Phys Chem. Comm.*, **9**, 359–363.
18. Frisch,C., Schreiber,G., Johnson,C.M. and Fersht,A.R. (1997) Thermodynamics of the interaction of barnase and barstar: changes in free energy versus changes in enthalpy on mutation. *J. Mol. Biol.*, **267**, 696–706.
19. Ladbury,J.E. and Chowdhry,B.Z. (1996) Sensing the heat: the application of isothermal titration calorimetry to thermodynamic studies of biomolecular interactions. *Chem. Biol.*, **3**, 791.
20. Berens,C., Thain,A. and Schroeder,R. (2001) A tetracycline-binding RNA aptamer Bioorg. *Med. Chem.*, **9**, 2549–2556.
21. Brodersen,D.E., Clemons,W.M.,Jr, Carter,A.P., Morgan-Warren,R.J., Wimberly,B.T. and Ramakrishnan,V. (2000) The structural basis for the action of the antibiotics tetracycline, pactamycin, and hygromycin B on the 30S ribosomal subunit. *Cell*, **103**, 1143–1154.
22. Pioletti,M., Schlunzen,F., Harms,J., Zarivach,R., Gluhmann,M., Avila,H., Bashan,A., Bartels,H., Auerbach,T., Jacobi,C. *et al.* (2001) Crystal structures of complexes of the small ribosomal subunit with tetracycline, edeine and IF3. *EMBO. J.*, **20**, 1829–1839.
23. Epe,B. and Woolley,P. (1984) The binding of 6-demethylchlortetracycline to 70S, 50S and 30S ribosomal particles: a quantitative study by fluorescence anisotropy. *EMBO J.*, **3**, 121–126.
24. Zuker,M. (2003) Mfold web server for nucleic acid folding and hybridization prediction. *Nucleic Acids Res.*, **31**, 3406–3415.